







## Article

# Optical Transmission Plasmonic Color Filter with Wider Color Gamut Based on X-Shaped Nanostructure

Rehan Shafiq <sup>1</sup>, Adnan Daud Khan <sup>2</sup>, Fatemah F. Al-Harbi <sup>3</sup>, Farman Ali <sup>4</sup>, Ammar Armghan <sup>5</sup>, Muhammad Asif <sup>6</sup>, Anees Ur Rehman <sup>1</sup>, Esraa Mousa Ali <sup>7</sup>, Farhad Arpanaei <sup>8</sup>, Mohammad Alibakhshikenari <sup>9</sup> and Mariana Dalarsson <sup>10,\*</sup>

- <sup>1</sup> Department of Electrical Engineering, Sarhad University of Science and Information Technology, Khyber Pukhtunkhwa, Peshawar 25220, Pakistan; rehanshafiq84@gmail.com (R.S.); anees.ee@suit.edu.pk (A.U.R.)
  - <sup>2</sup> Center for Advanced Studies in Energy, University of Engineering and Technology, Khyber Pukhtunkhwa, Peshawar 25124, Pakistan; adnan.daud@uetpeshawar.edu.pk
  - <sup>3</sup> Department of Physics, College of Science, Princess Nourah bint Abdulrahman University, P.O. Box 84428, Riyadh 11671, Saudi Arabia; ffarharbi@pnu.edu.sa
  - <sup>4</sup> Department of Electrical Engineering, Qurtuba University of Science and IT, Dera Ismail Khan 29050, Pakistan; drfarmanali.optics@qurtuba.edu.pk
  - <sup>5</sup> Department of Electrical Engineering, College of Engineering, Jouf University, Sakaka 72388, Saudi Arabia; aarmghan@ju.edu.sa
  - <sup>6</sup> Department of Electrical Engineering, Main Campus, University of Science & Technology, Bannu 28100, Pakistan; masifeed@ustb.edu.pk
  - <sup>7</sup> Faculty of Aviation Sciences, Amman Arab University, Amman 11953, Jordan; esraa\_ali@aau.edu.jo
  - <sup>8</sup> Department of Telematic Engineering, Universidad Carlos III de Madrid, 28911 Leganés, Madrid, Spain; farhad.arpanaei@uc3m.es
  - <sup>9</sup> Department of Signal Theory and Communications, Universidad Carlos III de Madrid, 28911 Leganés, Madrid, Spain; mohammad.alibakhshikenari@uc3m.es
  - <sup>10</sup> School of Electrical Engineering and Computer Science, KTH Royal Institute of Technology, 100-44 Stockholm, Sweden
- \* Correspondence: mardal@kth.se

**Citation:** Shafiq, R.; Khan, A.D.; Al-Harbi, F.F.; Ali, F.; Armghan, A.; Asif, M.; Rehman, A.U.; Ali, E.M.; Arpanaei, F.; Alibakhshikenari, M.; et al. Optical Transmission Plasmonic Color Filter with Wider Color Gamut Based on X-Shaped Nanostructure. *Photonics* **2022**, *9*, 209. <https://doi.org/10.3390/photonics9040209>

Received: 8 February 2022

Accepted: 17 March 2022

Published: 23 March 2022

**Publisher's Note:** MDPI stays neutral with regard to jurisdictional claims in published maps and institutional affiliations.



**Copyright:** © 2022 by the authors. Licensee MDPI, Basel, Switzerland. This article is an open access article distributed under the terms and conditions of the Creative Commons Attribution (CC BY) license (<https://creativecommons.org/licenses/by/4.0/>).

**Abstract:** Extraordinary Optical Transmission Plasmonic Color Filters (EOT-PCFs) with nanostructures have the advantages of consistent color, small size, and excellent color reproduction, making them a suitable replacement for colorant-based filters. Currently, the color gamut created by plasmonic filters is limited to the standard red, green, blue (sRGB) color space, which limits their use in the future. To address this limitation, we propose a surface plasmon resonance (SPR) color filter scheme, which may provide a RGB-wide color gamut while exceeding the sRGB color space. On the surface of the aluminum film, a unique nanopattern structure is etched. The nanohole functions as a coupled grating that matches photon momentum to plasma when exposed to natural light. Metals and surfaces create surface plasmon resonances as light passes through the metal film. The plasmon resonance wavelength can be modified by modifying the structural parameters of the nanopattern to obtain varied transmission spectra. The International Commission on Illumination (CIE 1931) chromaticity diagram can convert the transmission spectrum into color coordinates and convert the spectrum into various colors. The color range and saturation can outperform existing color filters.

**Keywords:** extraordinary optical transmission; plasmonic color filters; red, green, blue color gamut

## 1. Introduction

A color filter is a common optical device that is used to transmit or reflect light at a given wavelength in order to show the desired color in the desired manner. Anti-counterfeiting devices and techniques as well as display and imaging sensor manufacturers routinely employ color filters in their products [1,2]. When using conventional filters, the absorption of light with particular wavelengths and the display of particular colors is accomplished by the use of conventional pigments. Color filters made with traditional

chemical pigments will lose their effectiveness over time since they cannot tolerate high temperatures or UV light. Structural color filters have emerged in recent years as an alternative to classic color filters. To produce structural color, natural light interacts with micro-nanostructures and produces optical phenomena such as diffraction and scattering [3]. In contrast to chemical pigment, structural color has the advantages of non-fading, stable color, and environmental protection. These benefits of structural colors make researchers focus on the research of filters based on guided mode resonance [4], surface plasmon resonance [5,6], Mie resonance [7], or Fabry–Perot resonance. Plasmonic color filters are capable of achieving high resolutions and color adjustment, which is due to the smaller pixel sizes and changes in optical appearance of the plasmonic color filters used in specific applications. Some color filters, based on Fano resonance or Fabry–Perot cavity resonance, are highly scalable and easy to manufacture. However, their pixel size is undeniably smaller than a plasmonic color filter, and they have fewer opportunities to control the optical appearance. Despite this, plasmonic color filters have advantages in high-resolution applications [4]. In recent years, plasmonic color filters (PCFs) have received a lot of attention because of the extraordinary optical transmission (EOT) effect in metallic nanostructures. Plasmon oscillations are generated due to the interaction of electromagnetic fields and the conduction electrons in metals, and propagate along the metal surface. Surface plasmon polaritons (SPPs) are propagating surface plasmons that can bypass the usual diffraction limit and control light propagation at the subwavelength scale [5]. These SPPs improve light transmission when they are introduced into metal structures as periodic holes [2]. Localized surface plasmon resonances (LSPRs) can also play a role in the Extraordinary Optical Transmission (EOT) phenomena [8,9]. An EOT-like phenomenon is produced by the interaction of SPPs and LSPRs. A variety of factors influence the behavior of EOT [10,11], such as the form, size, hole arrangement, and dielectric used. This allows us to create new types of plasmonic nanostructures for controlling light at the nanoscale.

Experimental studies of the EOT effect in perforated metallic nanostructures have been conducted by many researchers. For example, Ranjith et al. suggested a plasma color filter that uses coaxial apertures and shows a single camera with a multispectral sensor using SPR and other effects [12]. The literature has previously reported the design of plasmonic color filters with a range of topologies. Ellenbogen et al., for example, created symmetric two connected slot nanoantennas with high transmission filters over the visible light spectrum [13]. Still, they could only filter out two types of light. A periodic subwavelength silver plasmonic color filter was proposed by Duempelmann et al. [14], but a good transmission was not achieved. Due to the insensitivity to polarization and incidence angles, a hexagonal array of coaxial aluminum holes was created as a viable filter [15,16]. Lin et al. [16] reported a high-transmission filter based on a multilayer thin-film Tamm plasma structure that can maintain the same perceived hue in the visible light spectrum throughout a wide variety of incidence angles.

Franklin et al. made a plasmonic system with modes that mixed in different directions between particles next to each other and their mirror counterparts using a large-area, repeatable, self-assembly method. In general, angle insensitivity is absent in hybridized modes [17]. Due to the polarization and incidence angle insensitivity, a metal–insulator–metal (MIM) plasma filter was developed by Liu et al. as a practical filter [18]. Su et al. produced a tapered aperture annular array made of metallic gold film perforated with silicon dioxide substrate, which promises an ideal filtering effect when tilted.

Structured colors and the broad color spectrum of RGB provide a great variety of pure spectral primary colors for practical applications [19]. It can store a more comprehensive range of color values than either the sRGB or Adobe RGB color spaces. Wide gamut RGB color spaces, on the other hand, cover 77.6% of the visible colors given by the CIE lab color spaces, whereas Adobe RGB color spaces only cover 52.1%, and sRGB color spaces just 35.9% [20]. The more intense the color displayed, the greater the saturation value in display or image, and as the color gamut is more comprehensive, the wider the variety of colors

represented. This is ideal, since the color filters have high color repetition, saturation, and purity as well as high contrast in a color filter. Peak intensity, spectral bandwidth, and full-width half-maximum (FWHM) are usually associated with these properties. Colors will appear brighter when the transmission intensity is higher. Light transmitted or reflected through existing plasmonic color filters, on the other hand, has a minimal color spectrum and saturation. Due to this problem, image quality suffers and restricts the future usage of plasmonic color filters.

We propose a structure for achieving EOT PCFs by introducing an asymmetric design in this paper. To the best of our knowledge, an asymmetric structure for broad mode EOT has never been thoroughly examined. Despite achieving significant transmission intensities, no attention has been paid to structure size. To put it simply, in order to obtain high transmission, the designer must increase the size of the hole or cavity, hence increasing the structure dimensions. In this paper, we provide concepts for achieving EOT by introducing an asymmetric framework. According to our understanding, asymmetric structures for broad mode EOT has not been completely explored earlier. This insight can also help to minimize the device's size. This discovery can also assist us in achieving a color RGB gamut that is super wide. Theoretically, we investigated a thin metallic aluminum (Al) film embedded with an X-shaped structure both symmetrically and asymmetrically based on the titanium dioxide (TiO<sub>2</sub>) substrate to obtain these observations. The optical properties and intensity distribution of the electric field of our proposed structure were analyzed using three-dimensional finite element methods. An ultra-wide color RGB gamut is produced via nearfield coupling and excitation of LSPRs, SPPs supported by holes. As a result of their effect on the charge distribution on metallic surfaces, the positioning and the intensity of an EOT peak can be customized by changing its structural properties. Our proposed structure's highly controllable EOT phenomena can produce an ultra-wide color RGB gamut in color filtering.

## 2. Structure and Computational Method

Figure 1 depicts the proposed perforated X-shaped nanostructure design, and the structure comprises an upper aluminum layer and a titanium dioxide substrate at the bottom. Both layers are held to a constant thickness of 50 nm. As shown in Figure 1b, a single unit cell structure consists of an X-shaped nanostructure hole embedded in the metal thin film with dimensions of L1 and L2 = 190 nm and W1 and W2 = 55 nm, where L1 and L2 represent the length of both cross arms of the X-shaped structure and W1 and W2 represent the width of both cross arms of the X-shaped design. The inclined angle of the X-shaped nanostructure is fixed at  $\theta = 45^\circ$ . Due to periodic boundary conditions, the unit cell has  $P_x = P_y = 350$  nm and is repeated along the  $x$ - and  $y$ -axes. An incident plane wave is perpendicular to the  $z$ -axis in the negative direction. Electric fields are polarized along the  $x$ -axis. The dielectric constant of aluminum is based on the data model of Johnson and Christy [21]. The medium around the structure is air, and all simulations are done using the finite element method in COMSOL Multiphysics Software (FEM). The mesh control method in the simulation is superb, and the mesh chooses free tetrahedral. The maximum and minimum cell sizes are 20 and 4 nanometers, respectively. Each aperture edge serves as a diffraction point where p-polarized light is coupled to SPPs whenever the light is incident onto a periodic aperture array. In the  $x$ - and  $y$ -directions, the lattice creates roughly the same amount of momentum as the array's periodicity. Due to the increased in-plane rate, light traveling freely along the metal–dielectric barrier is related to the SPP modes. As a result, the wave vector of the SPP can be expressed as follows [21]:

$$K_{spp} = \frac{2\pi}{\lambda} \sin\theta + mG_x + nG_y \quad (1)$$

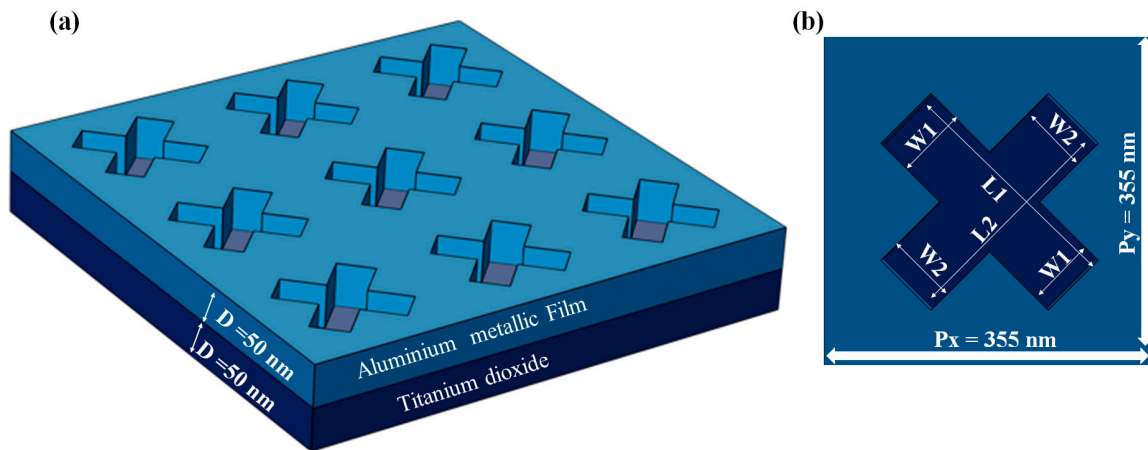


**Figure 1.** (a) EOT PCFs X-shaped nanostructure array; (b) a schematic illustration of the X-shaped structure of a single pixel. The filter’s substrate is TiO<sub>2</sub>, and an aluminum film is deposited on top of it.

The incident radiation’s wavelength is  $\lambda$ , the array’s angle of incidence is  $\theta$ , while  $m$  and  $n$  are integers determining the lattice vectors in the  $x$ - and  $y$ -directions, respectively with  $G_x = G_y = \frac{2\pi}{L}$  for a square array. The center peak position in a square lattice of square nanohole arrays can be calculated as follows [22]:

$$\lambda_{\max} = \frac{P}{\sqrt{i^2 + j^2}} \sqrt{\frac{\epsilon_d \epsilon_m}{\epsilon_d + \epsilon_m}} \tag{2}$$

Here,  $P$  is the array pitch, while  $\epsilon_d$ , and  $\epsilon_m$  are the dielectric constants of the dielectric and metal layers, respectively. The integers  $i$  and  $j$  signify the grating order, respectively. The position of the formant and the effect of splitting on it can be fine-tuned by changing the array of square nanoholes.

In order to evaluate the chromaticity of the transmissive spectrum in the 1931 Commission Internationale de L’Eclairage (CIE), the coordinate system values are calculated from the following expressions:

$$X = K \int R(\lambda) \bar{X}(\lambda) d\lambda \tag{3}$$

$$Y = K \int R(\lambda) \bar{Y}(\lambda) d\lambda \tag{4}$$

$$Z = K \int R(\lambda) \bar{Z}(\lambda) d\lambda \tag{5}$$

where  $R(\lambda)$  is the calculated spectrum and  $K$  is the correction factor. Here  $X$ ,  $Y$ , and  $Z$  denote the optical efficiency functions. The following is a formula for calculating the coordinate, and Figure 2 depicts the RGB, Adobe RGB, and sRGB chromatic gamut:

$$x = \frac{X}{X + Y + Z} \tag{6}$$

$$y = \frac{Y}{X + Y + Z} \tag{7}$$

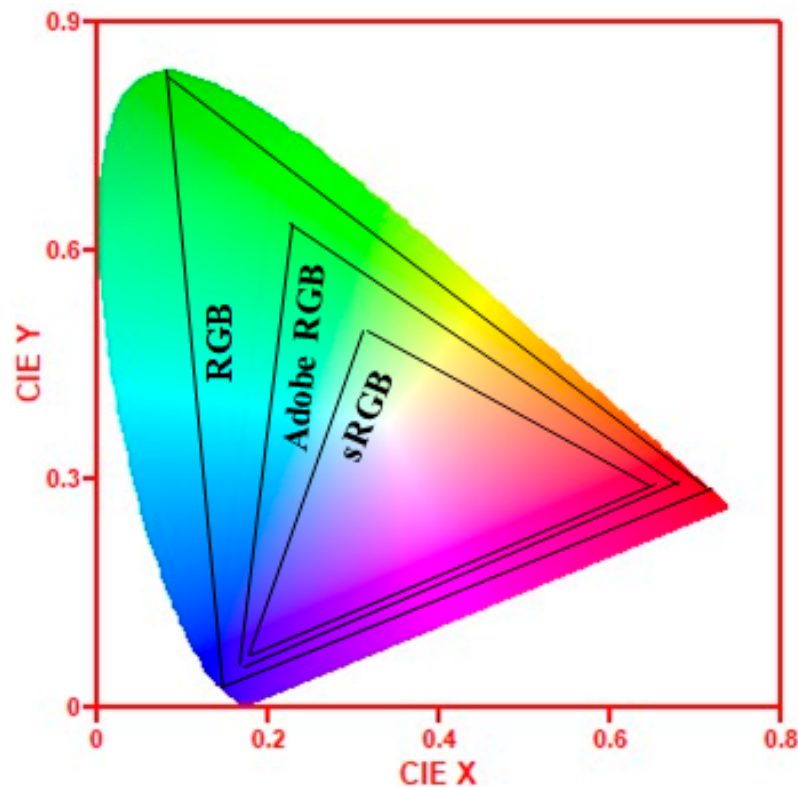


**Figure 2.** Three triangle chromaticity diagram of CIE 1931 showing the color gamut of RGB, Adobe RGB, and sRGB.

### 3. Results and Discussion

#### 3.1. Initial Extraordinary Optical Filter Transmission Plasmonic Color

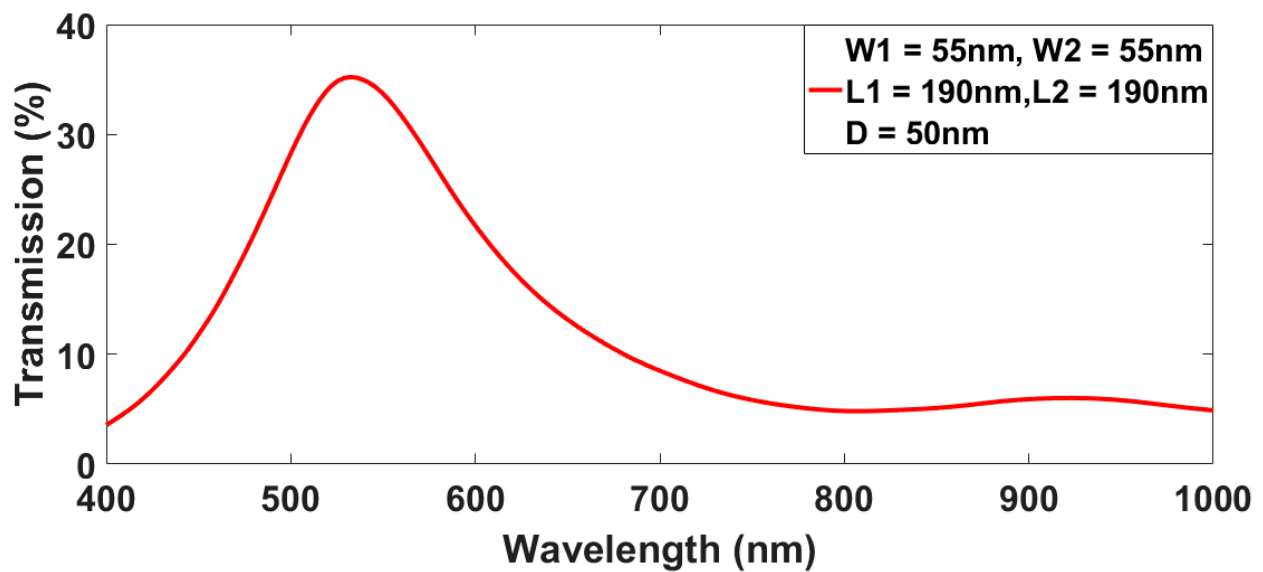
We studied the transmission spectra for initial EOT PCF, as shown in Figure 3a. We calculated the transmission spectra of the proposed structure using an X-shaped Al nanohole structure with  $W1$  and  $W2 = 55$  nm,  $L1$  and  $L2 = 190$  nm,  $D = 50$  nm, and  $Px$  and  $Py = 350$  nm as the initial PCF. At wavelength 518 nm, an enhanced broad transmission  $T = 40\%$  was noted. At the air–aluminum interface and the aluminum–titanium dioxide interface, respectively, transmission mode occurred. When surface plasmon resonance occurred, there was clear light confinement in the X-shaped nanostructure, as shown in Figure 3b, and transmission occurred in the visible light region, showing that the proposed structure is acceptable for the transmittive color filter. SPPs and LSPRs both contributed to the EOT phenomenon; in the case of similar energy levels, they became transmission conductive. As a result, LSPRs on metal surfaces [23] and SPPs on the metal surface [24] can be attributed to EOT occurrences.

The electric field intensity distributions are shown in Figure 3b to understand better the underlying physical principles. A significant portion of the field intensity was restricted to the Al structure’s edges and side surfaces, suggesting that LSPRs and SPPs were excited and linked to the Al film [25,26].

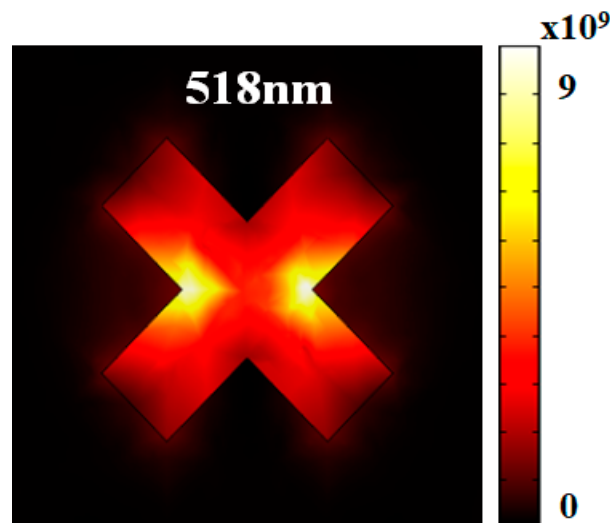
#### 3.2. Influence of the Film Thickness on Extraordinary Optical Transmission Plasmonic Color Filter

To better understand the proposed structure, we investigated the effects of thickness of the Al film  $D$  on transmission response. Figure 4 depicts the suggested structure’s transmission spectrum with varied  $D = 50$  nm, 75 nm, and 100 nm with fixed  $W1$  and  $W2 = 55$  nm,  $L1$  and  $L2 = 190$  nm, and  $P = 350$  nm. Metal thickness could thus be employed to adjust the X-shaped structure’s stability. With increasing  $D$ , the transmission peak red shifted slightly, as shown here when we increased the thickness from 50 nm to 100 nm; a modest reduction in transmission peak was also observed. When  $D$  was increased from

50 to 100 nm, the transmission peak centered at 518 nm ( $T = 34\%$ ) shifted to 532 nm ( $T = 15\%$ ). The resonance wavelength ranged between 518 nm and 532 nm. As a result, SPP resonance and LSPR excitation within the nanoholes may have been responsible for these resonant peaks. The deep cavity length was increased as  $D$  increased, and as a result, wavelengths were redshifted. The resonant characteristics can be determined from the equation  $kh = \pi(m + 1/2)$ , where  $k$  denotes the plasmon wavevector along the  $z$  axis,  $h$  denotes the hole height, and the resonance order is  $m = 0, 1, 2, \dots$ . The plasmon states that satisfy the resonance criterion in the preceding equation strongly couple to the incident light and have a higher transmission coefficient, resulting in maxima in the transmission spectrum.



(a)



(b)

**Figure 3.** (a) Calculated transmission spectra for initial EOT PCF; (b) electric field distribution at resonant peak.

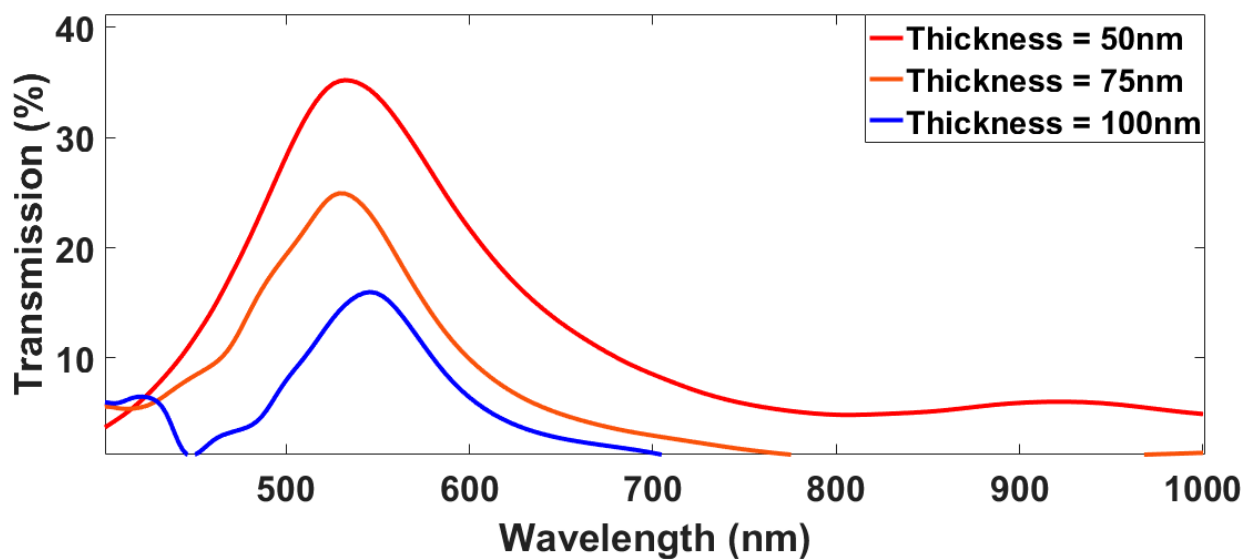


**Figure 4.** The transmission spectrums of the proposed structure with different thicknesses of Al were calculated.

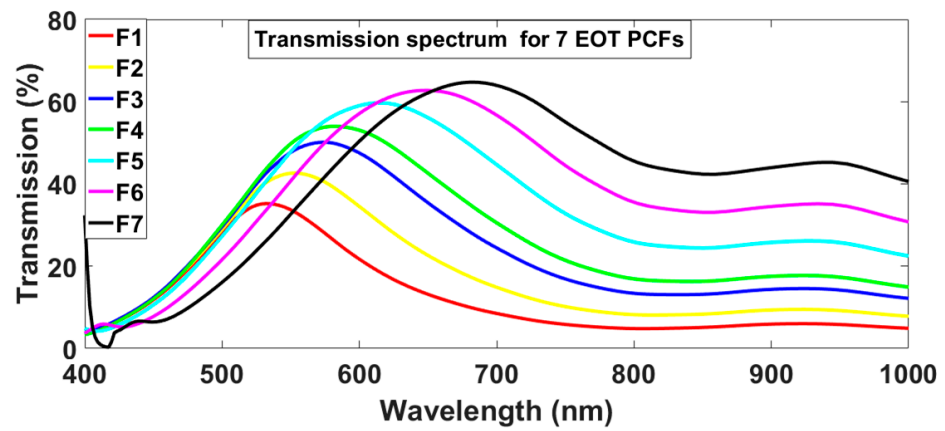
Furthermore, the resonant cavity is well known to rely on waveguides to facilitate the propagation of gap plasmon modes [27]. However, the desired application may require a compromise between stability and transmission. Compared to filters with high information but poor stability made from thinner metallic layers, thicker ones have better communication but lower instability. The thickness of the Al was fixed at 50 nm to achieve acceptable transmission of the following investigations when examining the other geometrical parameters.

Regarding the thickness indicated, it is noted that inappropriate experimental settings and a thinner metallic structure may result in fabrication problems. Regarding topologies that are easy to lift during fabrication, all recommended topologies were considered to have a minimum thickness of 50 nm. This is typical for fabricated plasmonic devices, with thicknesses ranging from 50 nm to 20 nm [28,29]. Plasmonic filters were created using two linked resonators with a coupling space of 5 nm. Similarly, the guides and resonators were separated by 5 nm [30]. A plasmonic-based sensor was developed using metallic structures with shorter distances [31]. Compared to the proposed layouts in this paper, such designs necessitate a higher level of fabrication precision. According to the previous study, the recommended structure may have feasible and suitable thicknesses for the manufacturing process.

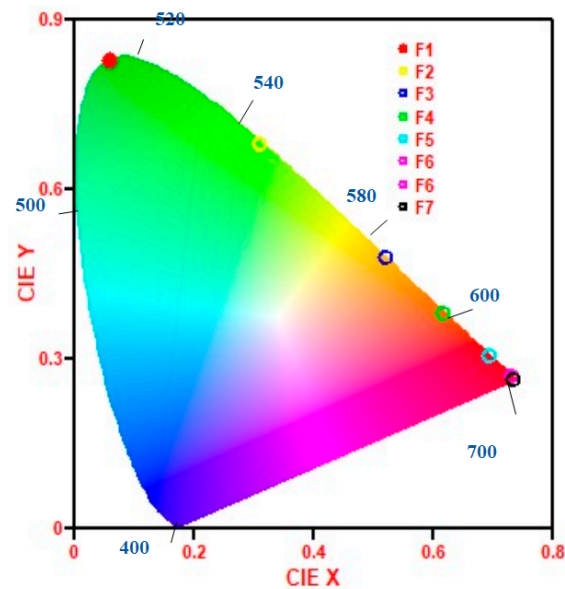
### 3.3. Influence of Width and Length (Symmetric Structure) on Extraordinary Optical Transmission Plasmonic Color Filter

As shown in Figure 5, we investigated the influence of the widths  $W_1$  and  $W_2$  and lengths  $L_1$  and  $L_2$  of both cross arms of the X-shaped nanostructure on transmission spectra. In Figure 5, we designed seven EOT PCFs, and we named them F1, F2, F3, F4, F5, F6, and F7, in which the widths  $W_1$  and  $W_2$  changed from 55 to 95 nm in 5 nm intervals, and the lengths  $L_1$  and  $L_2$  changed from 190 to 250 nm with 10 nm intervals. We increased widths and lengths symmetrically while the other parameters remained constant ( $D = 50$  nm and  $P_x$  and  $P_y = 350$  nm). F1 (red curve), F2 (brown curve), F3 (blue curve), F4 (green curve), F5 (cyan curve), F6 (magenta curve), and F7 (black curve) signified these seven EOT PCFs, as seen in Figure 5a. When  $W_1$ ,  $W_2$ , and  $L_1$ ,  $L_2$  increased from 55 to 95 nm and 190 to 250 nm, respectively, these seven EOT PCF transmission peaks exhibited a noticeable redshift from 518 nm (F1) to 552 nm (F2), 581 nm (F3), 598 nm (F4), 621 nm (F5), 654 nm (F6), and finally 703 nm (F7) in almost the same intervals of 30 nm. Furthermore, the intensity grew from  $T = 34\%$  to  $T = 65\%$ , while the bandwidth of the transmission peak became broader. The

resonant interaction of LSPRs and SPPs is strongly connected to these occurrences in our proposed structure.



(a)



(b)

**Figure 5.** (a) Calculated transmission spectrum obtained for 7 EOT PCFs by changing the width  $W_1$ ,  $W_2$  from 55 to 95 nm and length  $L_1$ ,  $L_2$  from 190 to 250 symmetrically. (b) Seven EOT PCFs chromaticity diagram of CIE 1931 showing color change when length and width of the X-shaped nanostructure changed symmetrically.

The X-shaped structure’s width and length were adjusted to provide a wide range of color gamuts. Then, as illustrated in Figure 5b, the chromaticity diagram coordinates were calculated from the obtained transmission spectrum, and then the color change on the chromaticity diagram CIE 1931 were observed.

Figure 6 shows the electric field intensity distributions of seven EOT PCFs with varied  $W_1$ ,  $W_2$ , and  $L_1$ ,  $L_2$  at the corresponding center wavelengths. In addition, the near-field interaction between the LSPR and SPPs on the Al film side surfaces may be related to the X-shaped nanostructure on its left and right edges. LSP and SPPs in the up and down hollow holes also exhibited weak interactions because of the weak electric field. The field intensity was restricted at two sides of the structure when  $W_1$ ,  $W_2$ , and  $L_1$ ,  $L_2$  increased, as shown in Figure 6, implying that the transmission peak in Figure 6 was redshifted due to more robust LSPRs in more robust localized waveguide resonances seen in Figure 5a. Exciting EOT in our proposed structure would be aided by LSPRs and SPPs: Excitation and Interaction.



Exciting waveguide resonances have also influenced EOT in hollow cavities [32]. LSPR resonances cause the hole shift and localized waveguide resonances as length and width vary, consistent with our transmission calculation results.

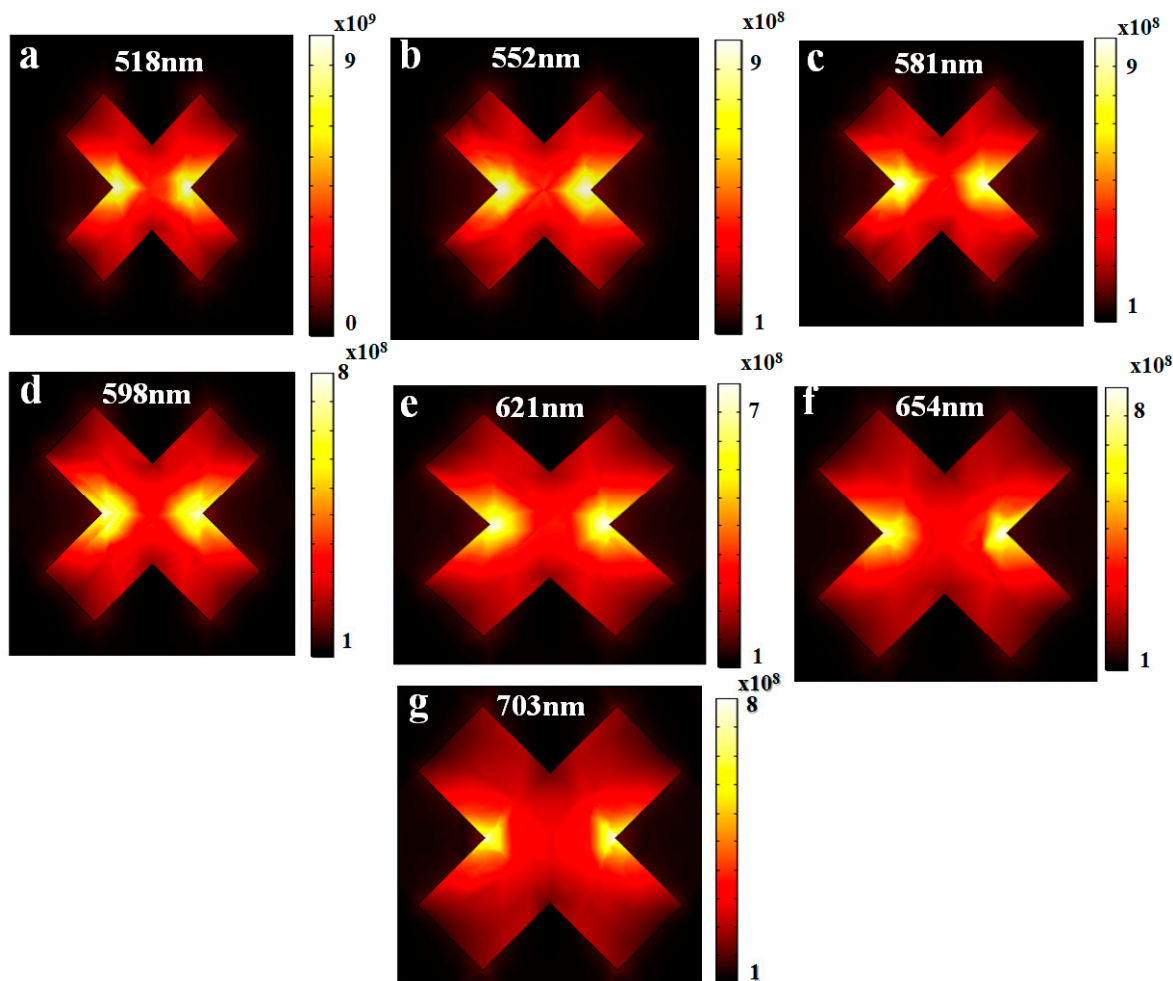


**Figure 6.** Electric field distribution for 7 EOT PCFs at wavelengths 518 nm (a), 552 nm (b), 581 nm (c), 598 nm (d), 621 nm (e), 654 nm (f), and 703 nm (g) by changing the width  $W_1, W_2$  from 55 to 95 nm and length  $L_1, L_2$  from 190 to 250 symmetrically.

### 3.4. Influence of Asymmetric Structure on Extraordinary Optical Transmission Plasmonic Color Filter

We looked into a defect in the X-shaped nanostructure. We increased the  $W_1$  of all seven EOT PCFs (F1, F2, F3, F4, F5, F6, and F7), as seen in Figure 5, and we added defects and named it the asymmetric X-shaped nanostructure. Schematic illustration and calculated transmission spectra of the defective structure are shown in Figures 7 and 8. In F1, we increased  $W_1$  from 55 to 85 nm with a 10 nm interval, and  $d_1$  represented the defect.  $W_1$  rose from 60 to 90 nm in F2, which  $d_2$  represented.  $W_1$  increased from 65 to 95 nm in F3, 70 to 100 nm in F4, 85 to 105 nm in F5, 90 to 110 nm in F6, and 95 to 115 nm in F7. We compared  $d_1$  to F1,  $d_2$  to F2,  $d_3$  to F3,  $d_4$  to F4,  $d_5$  to F5,  $d_6$  to F6, and  $d_7$  to F7 in Figure 8a–g. With increasing  $W_1$ , the transmission peak blue shifted noticeably, accompanied by a modest rise in the transmission peak’s strength. Table 1 shows the wavelength and transmission intensities of all the heights achieved in Figure 8a–g. LSPRs explain the proposed shaped nanoholes and SPPs in Al films. Furthermore, increasing  $W_1$  reduced the confinement of LSPRs in nanoholes, and the SPP wavelength was lowered in a single wavelength of excitation.

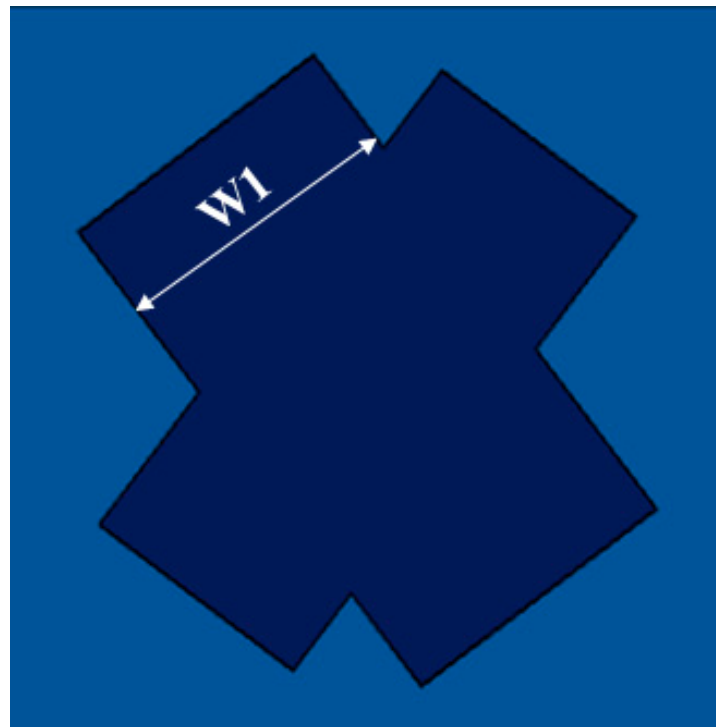


**Figure 7.** Asymmetric X shaped nanostructure.

**Table 1.** Asymmetric structure.

Seven Extraordinary Optical Transmission Plasmonic Color Filter	Wavelength Shifts in Defects (d1–d7)	Transmission
F1 = 518 nm, T = 34%	d1 = 502 nm	36%
	d1 = 488 nm	38%
	d1 = 474 nm	40%
F2 = 552 nm, T = 38%	d2 = 525 nm	41%
	d2 = 519 nm	44%
	d2 = 503 nm	46%
F3 = 581 nm, T = 44%	d3 = 555 nm	48%
	d3 = 547 nm	50%
	d3 = 543 nm	52%
F4 = 598 nm, T = 50%	d4 = 571 nm	55%
	d4 = 560 nm	58%
	d4 = 542 nm	60%
F5 = 621 nm, T = 56%	d5 = 599 nm	61%
	d5 = 587 nm	63%
	d5 = 575 nm	65%
F6 = 654 nm, T = 62%	d6 = 635 nm	64%
	d6 = 625 nm	66%
	d6 = 616 nm	68%
F7 = 703 nm, T = 66%	d7 = 686 nm	66%
	d7 = 670 nm	67%
	d7 = 657 nm	69%

The predicted electric field distribution defective (asymmetric) structure that we achieved in Figure 8a–g is depicted in Figures 9–15. In Figures 9–15, the Al nanostructure is characterized by a strong electric field around its edges, centered around a relatively low electric field. Therefore, the length of the hole has a significant impact on EOT. In

certain phases of the hole, dispersion of SPPs is required. Increased  $W1$  reduces the confinement of LSPRs in nanoholes, lowering the wavelength of SPPs in one particular excitation wavelength. Excited waveguide resonances have also influenced EOT in hollow cavities. When the width of the X-shaped nanostructure is changed, a localized waveguide resonance and the resonant frequency of LSPRs are excited in the hole, correlating with our transmission calculation results to produce higher transmission.

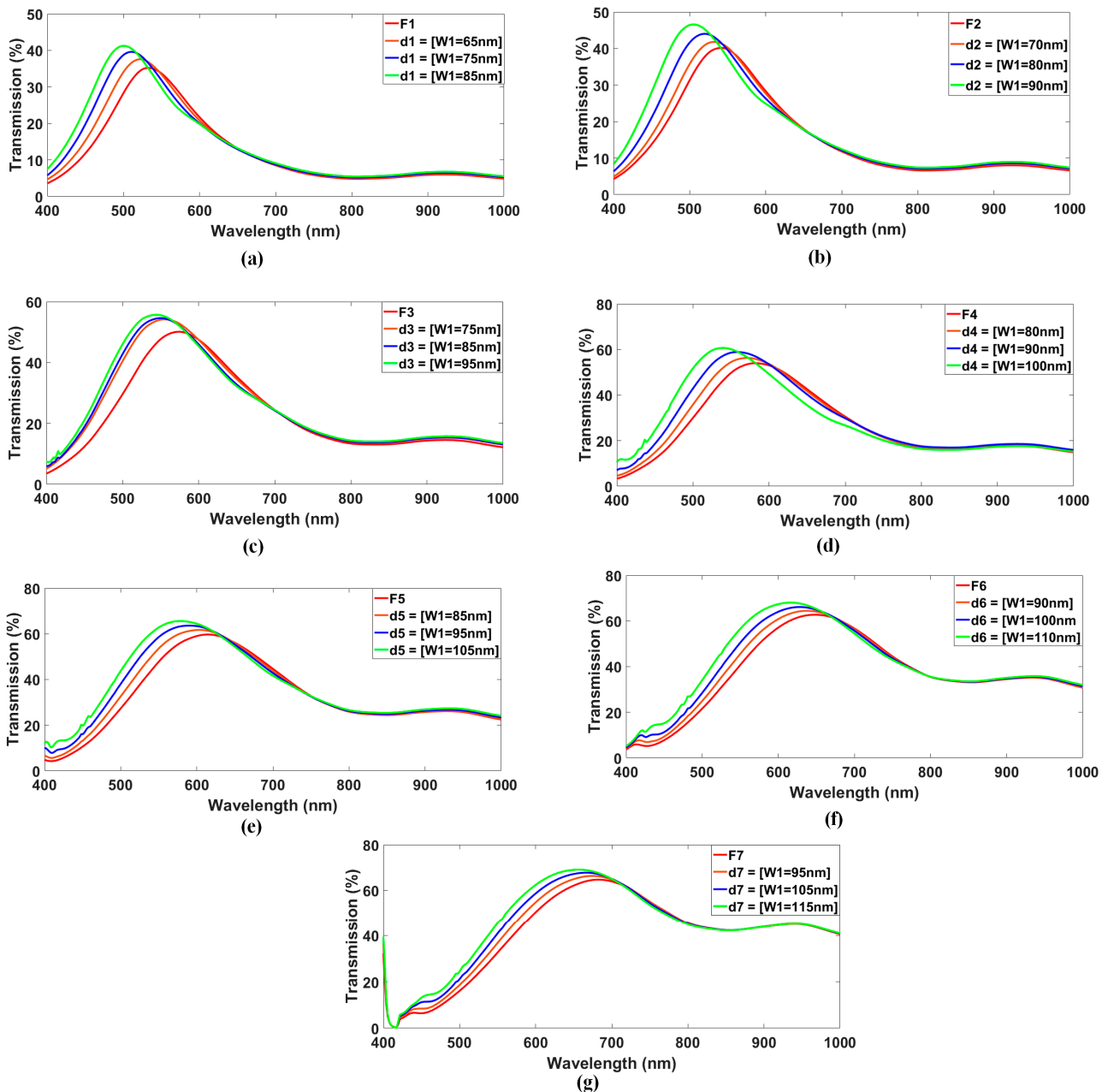


**Figure 8.** Calculated transmission spectra defective (asymmetric) structure by changing the width  $W1$  of 7 EOT PCFs and representing the defect by  $d1$ ,  $d2$ ,  $d3$ ,  $d4$ ,  $d5$ ,  $d6$ , and  $d7$ . (a)  $F1$  compared with  $d1$ , (b)  $F2$  compared with  $d2$ , (c)  $F3$  compared with  $d3$ , (d)  $F4$  compared with  $d4$ , (e)  $F5$  compared with  $d5$ , (f)  $F6$  compared with  $d6$ , and (g)  $F7$  compared with  $d7$ .

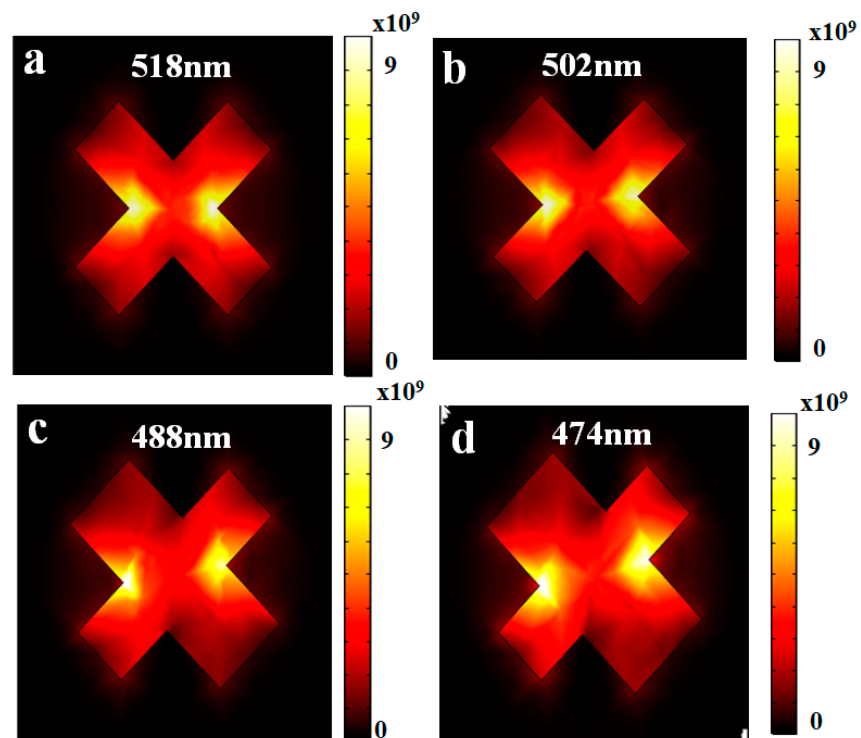


**Figure 9.** Electric field distribution at wavelengths 518 nm (a), 502 nm (b), 488 nm (c), and 474 nm (d) for defective structure d1.

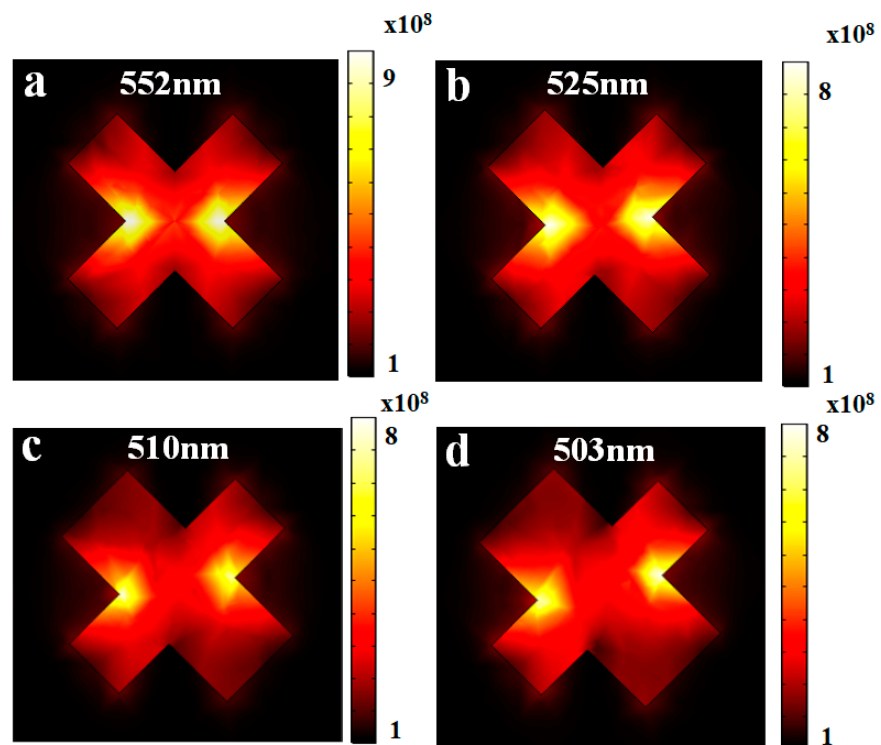


**Figure 10.** Electric field distribution at wavelengths 552 nm (a), 525 nm (b), 510 nm (c), and 503 nm (d) for defective structure d2.

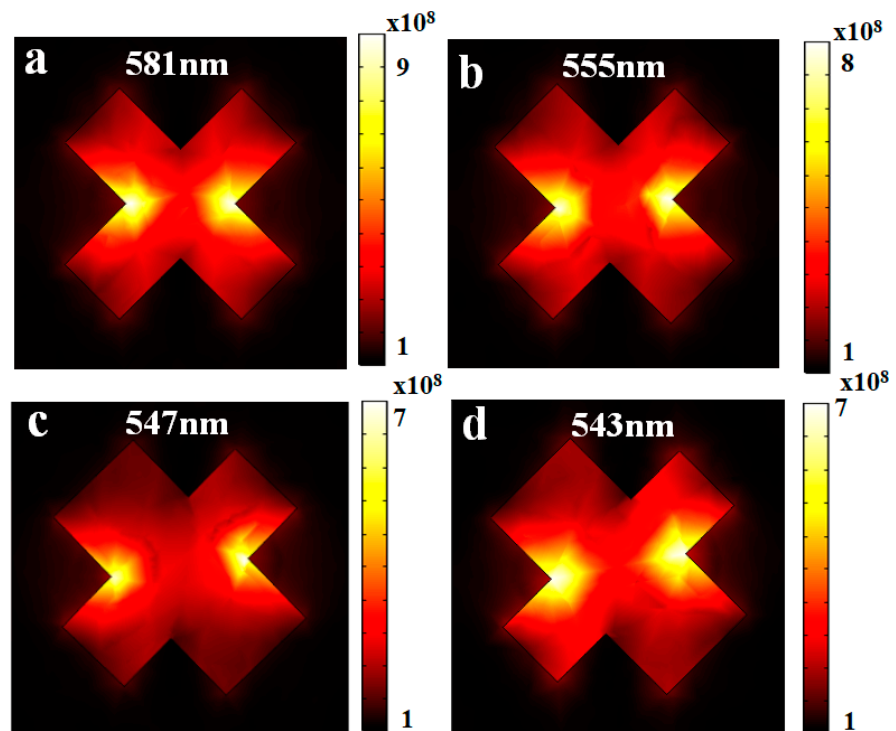


**Figure 11.** Electric field distribution at wavelengths 581 nm (a), 555 nm (b), 547 nm (c), and 543 nm (d) for defective structure d3.

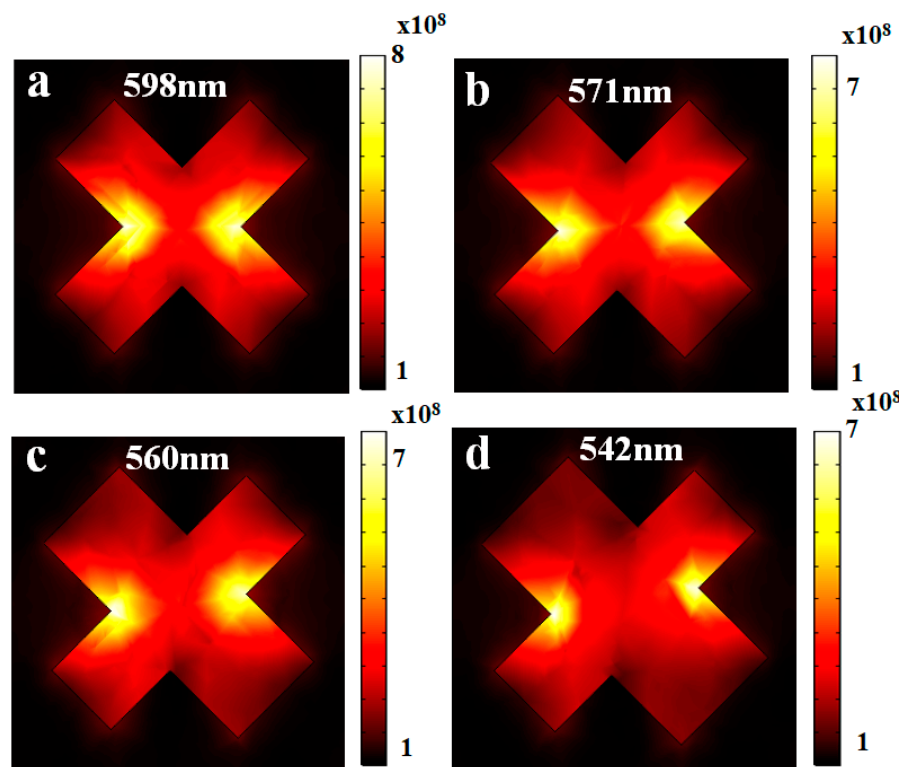


**Figure 12.** Electric field distribution at wavelengths 598 nm (a), 571 nm (b), 560 nm (c), and 542 nm (d) for defective structure for d4.

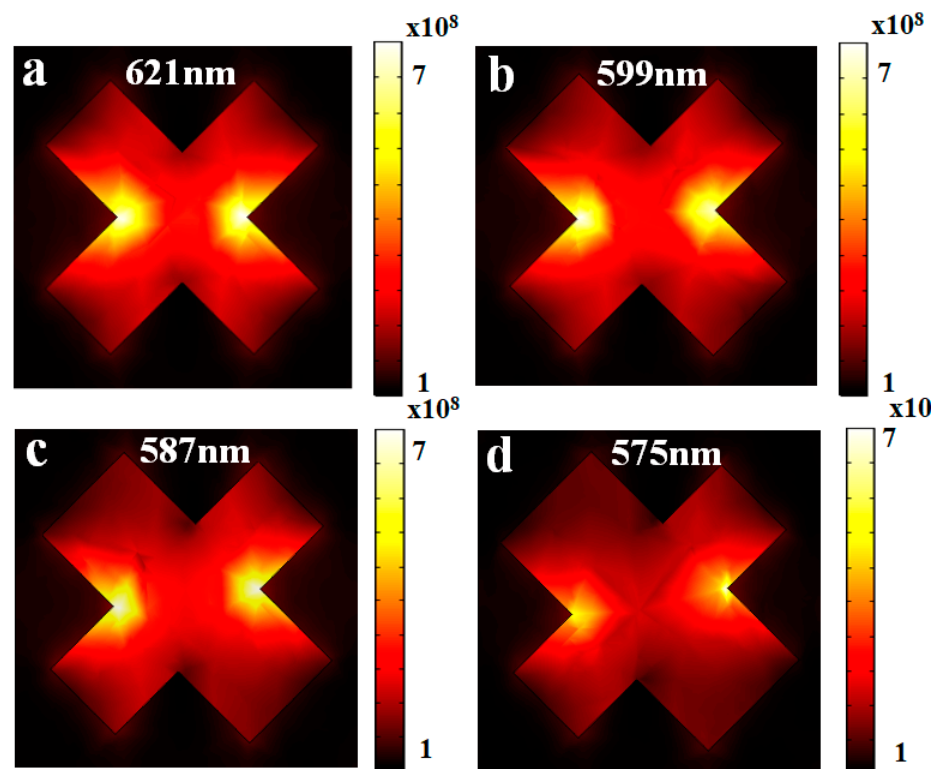


Figure 13. Electric field distribution at wavelengths 621 nm (a), 599 nm (b), 587 nm (c), and 575 nm (d) for defective structure for d5.

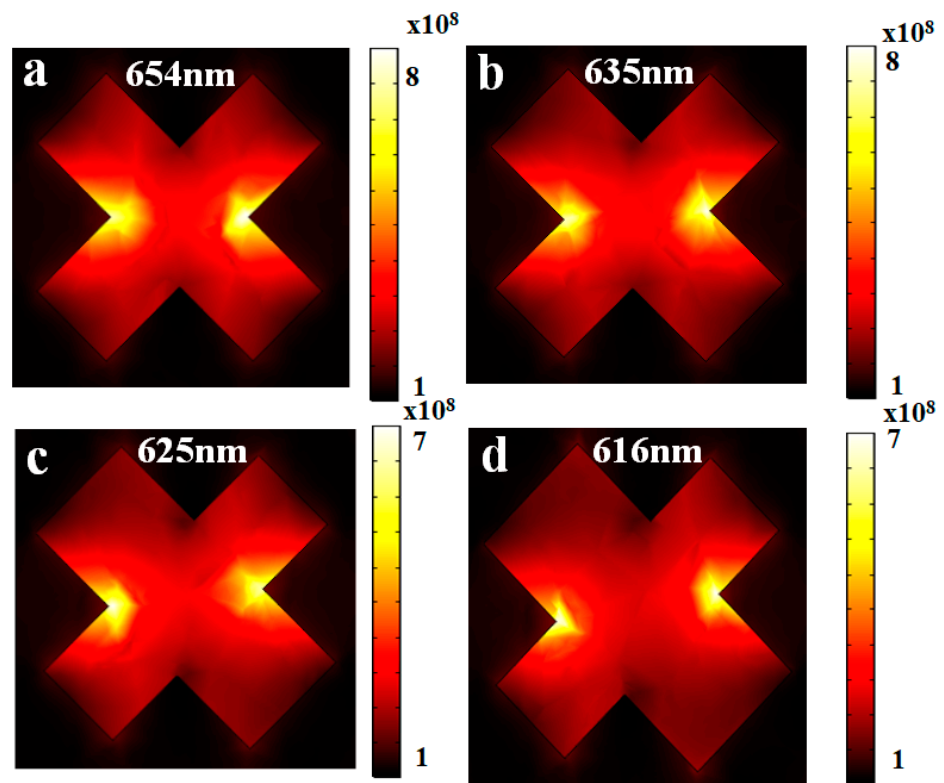
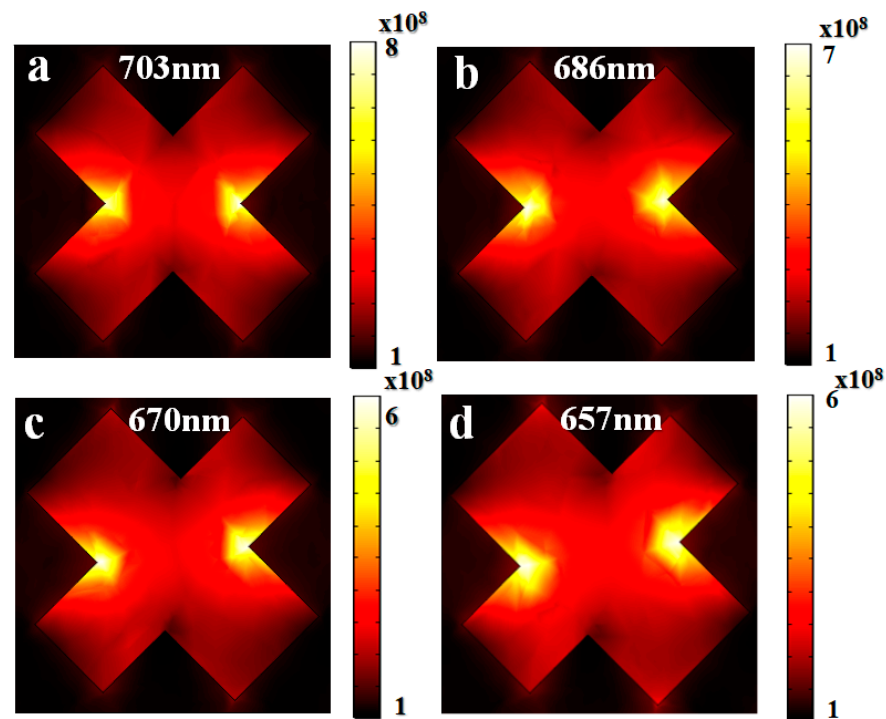


Figure 14. Electric field distribution at wavelengths 654 nm (a), 635 nm (b), 625 nm (c), and 616 nm (d) for defective structure for d6.



**Figure 15.** Electric field distribution at wavelengths 703 nm (a), 686 nm (b), 670 nm (c), and 657 nm (d) for defective structure for d7.

A color gamut that covers a broad spectrum was obtained by changing the width  $W1$  of the X-shaped nanostructure. The resulting transmission spectrum was computed to obtain the chromaticity diagram coordinates, as shown in Figure 16a–g.

Table 2 compares the results of our proposed structure to recently proposed similar structures in the literature. Our results show the broad spectrum RGB, which provides a great variety of pure spectral primary colors. To determine the RGB color from our proposed structure, we used the best scenarios for RGB colors, specifically 474 nm,  $T = 40\%$  from d1, and the structural parameters for blue were  $W1 = 85$  nm,  $W2 = 55$  nm,  $L1 = 190$  nm,  $L2 = 190$  nm, 525 nm, and  $T = 41\%$  from d2; for pure green the parameter is  $W1 = 70$  nm,  $W2 = 60$  nm,  $L1$  and  $L2 = 210$  nm, and 684 nm  $T = 66\%$  from d7; for deep red, structural parameters are as follows:  $W1 = 115$  nm,  $W2 = 95$  nm,  $L1$  and  $L2 = 250$  nm, as shown in Figure 17a. The CIE 1931 chromaticity diagram depicts the spectrum data generated via simulation, and is shown in Figure 17b, to visualize the filter-induced changes to colors. The illustration demonstrates that the system we developed can provide red, green, and blue filtration. The black triangle represents the primary red, green, and blue color scheme (RGB). The RGB color space is the most extensively used color system in the world.

**Table 2.** Comparison with other recently reported plasmonic color filters.

References	Structure Type	Material	Color Gamut
[32]	Square array	Aluminum	sRGB
[33]	Circular array	Multilayer zinc sulphide and silver	sRGB
[34]	Square array	Silicon nitride	sRGB
[35]	Circular array	Aluminum and indium tin oxide	sRGB
[36]	Cross shaped with four rectangular edges	Silver and silicon dioxide	sRGB
[37]	Bowtie structure	Silver and silicon dioxide	sRGB
This study	X-shaped nanostructure	Aluminum and titanium dioxide	RGB

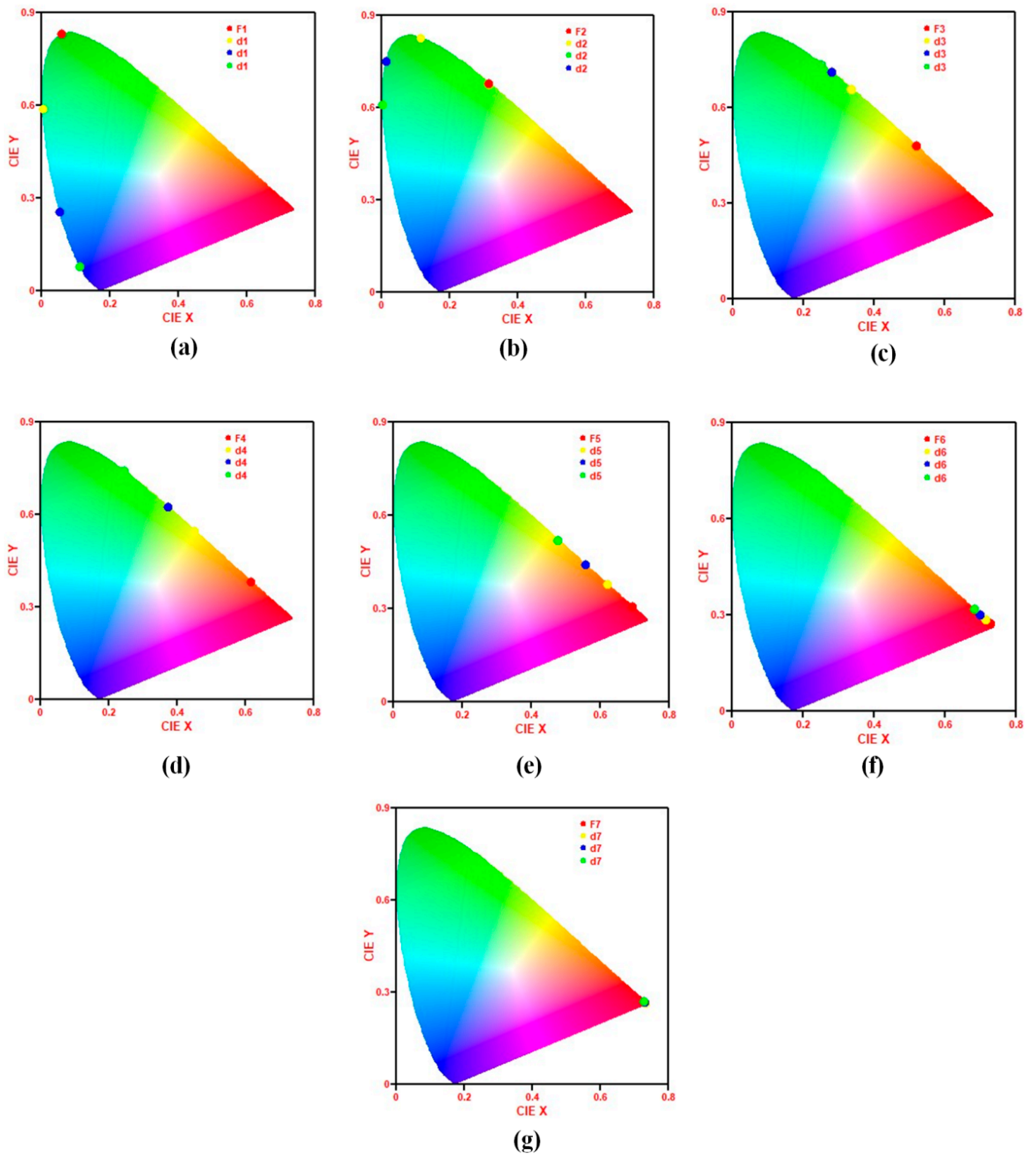
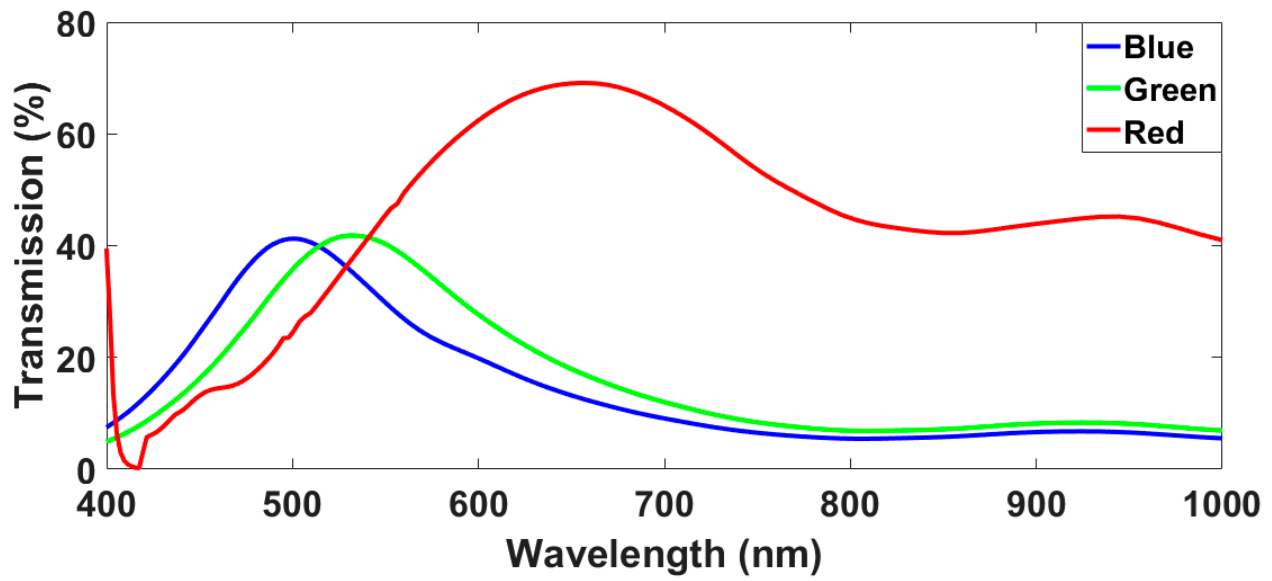
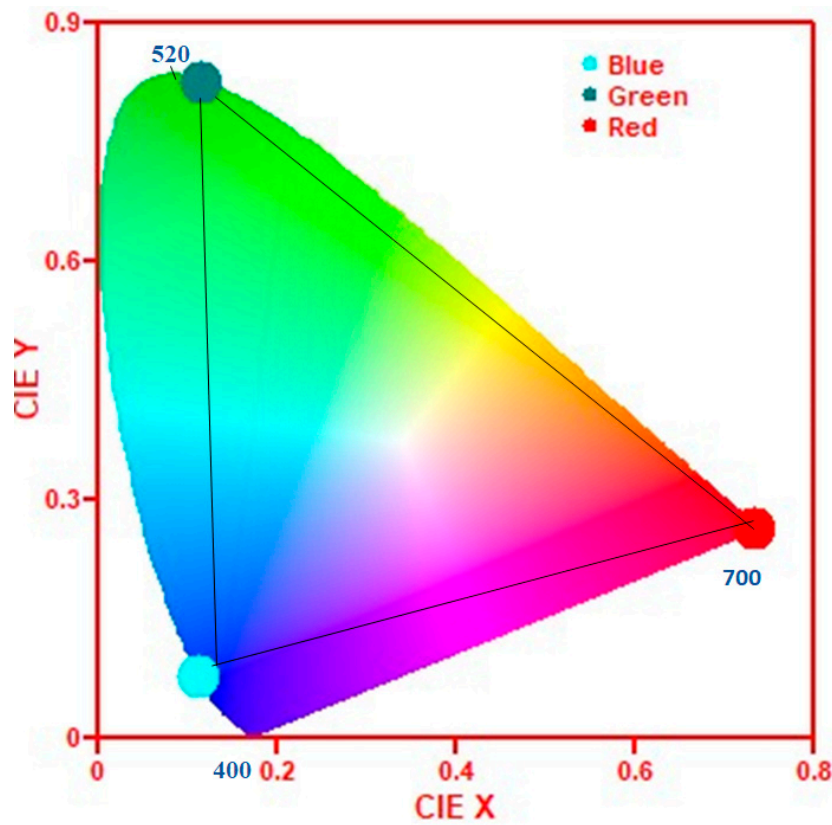


**Figure 16.** (a–g) Chromaticity diagram from CIE 1931 shows a shift in color when the width  $W_1$  of the X-shaped nanostructure is changed asymmetrically.





(a)



(b)

**Figure 17.** (a) Transmission spectrum of the structures that correspond to  $W1 = 85$  nm,  $W2 = 55$  nm,  $L1 = 190$  nm, and  $L2 = 190$  nm; the green-related structural parameters  $W1 = 70$  nm,  $W2 = 60$  nm,  $L1$  and  $L2 = 210$  nm; structures with red spectral lines in their structural characteristics  $W1 = 115$  nm,  $W2 = 95$  nm,  $L1$  and  $L2 = 250$  nm. (b) The CIE 1931 chromaticity diagram shows the color coordinates.

#### 4. Conclusions

This work proposed and investigated an Extraordinary Optical Transmission Plasmonic Color Filter using an X-shaped etched structure on an aluminum film based on

surface plasmon resonance. According to the experimental results, the design of the nanopattern and the aluminum layer's thickness can modify the metal's plasmon resonance. The experimental results reveal that changing the structural properties of the nanopattern and the aluminum film thickness can affect the resonance of plasmons on metal surfaces. The proposed color filter is designed to go beyond sRGB color spaces and can produce a wider RGB color gamut than existing surface plasmon filters. The proposed filter can deliver rich color filters with surface plasmon resonance and better picture quality than current color filters. The color range is more comprehensive, and the saturation levels are higher than current color filters. Therefore, the proposed filter may have applications in optical imaging, CMOS sensors, and photodetection.

**Author Contributions:** Conceptualization, R.S., A.A., F.F.A.-H., M.A. (Muhammad Asif), M.A. (Mohammad Alibakhshikenari) and M.D.; methodology, F.A. (Farman Ali), E.M.A., F.A. (Farhad Arpanaei), M.A. (Mohammad Alibakhshikenari), and M.D.; software, R.S., F.A. (Farman Ali), and A.A.; validation, R.S., A.U.R., F.F.A.-H., A.A., A.D.K., F.A. (Farhad Arpanaei), M.A. (Mohammad Alibakhshikenari), and M.D.; formal analysis, R.S., F.A. (Farhad Arpanaei), M.A. (Mohammad Alibakhshikenari), and M.D.; investigation, A.U.R., F.A. (Muhammad Asif), F.A. (Farman Ali), E.M.A., F.A. (Farhad Arpanaei), M.A. (Mohammad Alibakhshikenari), and M.D.; resources, R.S., A.A., and F.A. (Farman Ali); data curation, F.A. (Farman Ali), M.A. (Muhammad Asif), E.M.A., M.A. (Mohammad Alibakhshikenari), and M.D.; writing—original draft preparation, R.S., and F.A. (Farman Ali); writing—review and editing, A.D.K., F.A. (Farman Ali), A.A., E.M.A., F.A. (Farhad Arpanaei), M.A. (Mohammad Alibakhshikenari), and M.D.; visualization, M.A. (Muhammad Asif), E.M.A., F.A. (Farhad Arpanaei), M.A. (Mohammad Alibakhshikenari), and M.D.; supervision, F.F.A.-H., F.A. (Farman Ali), M.A. (Muhammad Asif), M.A. (Mohammad Alibakhshikenari) and M.D.; project administration, M.A. (Muhammad Asif), A.A. and F.A. (Farman Ali); funding acquisition, M.A. (Muhammad Asif), M.A. (Mohammad Alibakhshikenari) and M.D. All authors have read and agreed to the published version of the manuscript.

**Funding:** This project has received funding from Universidad Carlos III de Madrid and the European Union's Horizon 2020 research and innovation programme under the Marie Skłodowska-Curie Grant 801538.

**Institutional Review Board Statement:** Not applicable.

**Informed Consent Statement:** Not applicable.

**Data Availability Statement:** All data are included within the manuscript.

**Acknowledgments:** The authors sincerely appreciate the support from Universidad Carlos III de Madrid and the European Union's Horizon 2020 research and innovation programme under the Marie Skłodowska-Curie Grant 801538.

The authors express their gratitude to Princess Nourah bint Abdulrahman University Researchers Supporting Project (Grant No. PNURSP2022R55), Princess Nourah bint Abdulrahman University, Riyadh, Saudi Arabia.

**Conflicts of Interest:** The authors declare no conflict of interest.

## References

1. Gu, Y.L.; Zhang, J.K.; Yang, S.P.; Yeo, C.-W.; Qiu, J.N. Color generation via subwavelength plasmonic nanostructures. *Nanoscale* **2015**, *7*, 6409–6419. [[CrossRef](#)] [[PubMed](#)]
2. Collison, R.; Pérez-Sánchez, J.B.; Du, M.; Trevino, J.; Yuen-Zhou, J.; O'Brien, S.; Menon, V.M. Purcell Effect of Plasmonic Surface Lattice Resonances and Its Influence on Energy Transfer. *ACS Photonics* **2021**, *8*, 2211–2219. [[CrossRef](#)]
3. Castro-Chacón, J.H.; Torres-Torres, C.; Khomenko, A.V.; García-Zárate, M.A.; Trejo-Valdez, M.; Martínez-Gutiérrez, H.; Torres-Martínez, R. Encryption of nonlinear optical signals in ZnO:Al thin films by ultrashort laser pulses. *J. Mod. Opt.* **2017**, *64*, 601–608. [[CrossRef](#)]
4. Raj Shrestha, V.; Lee, S.S.; Kim, E.S.; Choi, D.Y. Polarization-tuned dynamic color filters incorporating a dielectric-loaded aluminum nanowire array. *Sci. Rep.* **2015**, *5*, 12450. [[CrossRef](#)] [[PubMed](#)]
5. Gramotnev, D.K.; Bozhevolnyi, S.I. Plasmonics beyond the diffraction limit. *Nat. Photon* **2010**, *4*, 83–91. [[CrossRef](#)]
6. Lee, G.Y.; Yoon, G.; Lee, S.Y.; Yun, H.; Cho, J.; Lee, K.; Kim, H.; Rho, J.; Lee, B. Complete amplitude and phase control of light using broadband holographic metasurfaces. *Nanoscale* **2018**, *10*, 4237–4245. [[CrossRef](#)]

7. Zeng, B.; Gao, Y.; Bartoli, F.J. Ultrathin nanostructured metals for highly transmissive plasmonic subtractive color filters. *Sci. Rep.* **2013**, *3*, 2840. [[CrossRef](#)] [[PubMed](#)]
8. Deng, Y.; Cao, G.; Wu, Y.; Zhou, X.; Liao, W. Theoretical description of dynamic transmission characteristics in MDM waveguide aperture-side-coupled with ring cavity. *Plasmonics* **2015**, *10*, 1537–1543. [[CrossRef](#)]
9. Deng, Y.; Cao, G.; Yang, H.; Zhou, X.; Wu, Y. Dynamic control of double plasmon-induced transparencies in aperture-coupled waveguide-cavity system. *Plasmonics* **2018**, *13*, 345–352. [[CrossRef](#)]
10. Zheng, Z.; Zheng, Y.; Luo, Y.; Yi, Z.; Zhang, J.; Liu, Z.; Yang, W.; Yu, Y.; Wu, X.; Wu, P. A switchable terahertz device combining ultra-wideband absorption and ultra-wideband complete reflection. *Phys. Chem. Chem. Physics* **2022**, *24*, 2527–2533. [[CrossRef](#)] [[PubMed](#)]
11. Wu, X.; Zheng, Y.; Luo, Y.; Zhang, J.; Yi, Z.; Wu, X.; Cheng, S.; Yang, W.; Yu, Y.; Wu, P. A four-band and polarization-independent BDS-based tunable absorber with high refractive index sensitivity. *Phys. Chem. Chem. Physics* **2021**, *23*, 26864–26873. [[CrossRef](#)] [[PubMed](#)]
12. Ellenbogen, T.; Seo, K.; Crozier, K.B. Chromatic plasmonic polarizers for active visible color filtering and polarimetry. *Nano Lett.* **2012**, *12*, 1026–1031. [[CrossRef](#)]
13. Duempelmann, L.; Luu-Dinh, A.; Gallinet, B.; Novotny, L. Four-fold color filter based on plasmonic phase retarder. *ACS Photonics* **2016**, *3*, 190–196. [[CrossRef](#)]
14. He, X.; Beckett, P.; Unnithan, R.R. Transmission Enhancement in Coaxial Hole Array Based Plasmonic Color Filters. In *Multispectral Image Sensors Using Metasurfaces. Progress in Optical Science and Photonics*; Springer: Singapore, 2021; Volume 17. [[CrossRef](#)]
15. Lin, J.; Luo, S.; Zuo, D.; Wang, X. Multilayer structure for highly transmissive angle-tolerant color filter. *Opt. Commun.* **2018**, *427*, 158–162. [[CrossRef](#)]
16. Rajasekharan, R.; Dai, Q.; Wilkinson, T.D. Electro-optic characteristics of a transparent nanophotonic device based on carbon nanotubes and liquid crystals. *Appl. Opt.* **2010**, *49*, 2099–2104. [[CrossRef](#)] [[PubMed](#)]
17. Song, C.; Feng, Y.; Bao, Z.; Liu, G.; Wang, J.J.P. Angle-insensitive color filters based on multilayer ultrathin-film structures. *Plasmonics* **2020**, *15*, 255–261. [[CrossRef](#)]
18. Kinoshita, J.; Takamori, A.; Yamamoto, K.; Kuroda, K.; Suzuki, K. Measurement and analysis of color shift behavior at image pattern edges projected by raster-scan RGB mobile laser projectors. *Opt. Rev.* **2021**, 1–12. [[CrossRef](#)]
19. Suzuki, K.; Kubota, S. Understanding the exposure-time effect on speckle contrast measurements for laser displays. *Opt. Rev.* **2018**, *25*, 131–139. [[CrossRef](#)]
20. Wang, Y.; Duan, G.; Zhang, L.; Ma, L.; Zhao, X.; Zhang, X.J.S.R. Terahertz dispersion characteristics of super-aligned multi-walled carbon nanotubes and enhanced transmission through subwavelength apertures. *Sci. Rep.* **2018**, *8*, 2087. [[CrossRef](#)]
21. Su, J.; Wang, L.; Yang, J.; Kong, L.; Mo, X.; Lv, J.J.O.C. High selectivity plasmonic color filters based on tapered annular aperture arrays. *Opt. Commun.* **2020**, *475*, 126206. [[CrossRef](#)]
22. Zhu, R.; Chen, L.; Zong, Z.; Tang, Z.; Qian, J.; Tang, S.; Du, Y. Tuning the shape of magneto-optical Kerr spectrum by changing the strip width in one-dimensional Ag-Co-Ag magnetoplasmonic nanogratings. *Appl. Phys. Lett.* **2019**, *115*, 072405. [[CrossRef](#)]
23. Rakhshani, M.R.; Mansouri-Birjandi, M.A.J.S.; Chemical, A.B. High sensitivity plasmonic refractive index sensing and its application for human blood group identification. *Sens. Actuators B Chem.* **2017**, *249*, 168–176. [[CrossRef](#)]
24. Rakhshani, M.R.; Mansouri-Birjandi, M.A.J.P. Utilizing the metallic nano-rods in hexagonal configuration to enhance sensitivity of the plasmonic racetrack resonator in sensing application. *Plasmonics* **2017**, *12*, 999–1006. [[CrossRef](#)]
25. Khani, S.; Danaie, M.; Rezaei, P. Tunable single-mode bandpass filter based on metal-insulator-metal plasmonic coupled U-shaped cavities. *IET Optoelectron.* **2019**, *13*, 161–171. [[CrossRef](#)]
26. Rakhshani, M.R.; Tavousi, A.; Mansouri-Birjandi, M.A. Design of a plasmonic sensor based on a square array of nanorods and two slot cavities with a high figure of merit for glucose concentration monitoring. *Appl. Opt.* **2018**, *57*, 7798–7804. [[CrossRef](#)]
27. Shabani, A.; Nezhad, M.K.; Rahmani, N.; Roknabadi, M.R.; Behdani, M.; Sanyal, B.J.P. Optical properties of Audoped titanium nitride nanostructures: A Connection between density functional theory and finite-difference time-domain method. *Plasmonics* **2019**, *14*, 1871–1879. [[CrossRef](#)]
28. Bora, M.; Fasenfest, B.J.; Behymer, E.M.; Chang, A.S.; Nguyen, H.T.; Britten, J.A.; Larson, C.C.; Chan, J.W.; Miles, R.R.; Bond, T.C. Plasmon resonant cavities in vertical nanowire arrays. *Nano Lett.* **2010**, *10*, 2832–2837. [[CrossRef](#)]
29. Wang, W.; Zhao, D.; Chen, Y.; Gong, H.; Chen, X.; Dai, S.; Yang, Y.; Li, Q.; Qiu, M. Grating-assisted enhanced optical transmission through a seamless gold film. *Opt. Express* **2014**, *22*, 5416–5421. [[CrossRef](#)]
30. Chowdhury, S.N.; Nyga, P.; Kudyshev, Z.A.; Garcia Bravo, E.; Lagutchev, A.S.; Kildishev, A.V.; Shalaev, V.M.; Boltasseva, A. Lithography-Free Plasmonic Color Printing with Femtosecond Laser on Semicontinuous Silver Films. *ACS Photonics* **2021**, *8*, 521–530. [[CrossRef](#)]
31. Liu, X.; Fu, G.; Liu, M.; Liu, G.; Liu, Z. High-Quality Plasmon Sensing with Excellent Intensity Contrast by Dual Narrow-Band Light Perfect absorbers. *Plasmonics* **2017**, *12*, 65–68. [[CrossRef](#)]
32. Shrestha, V.R.; Lee, S.S.; Kim, E.S.; Choi, D.Y. Aluminum plasmonics based highly transmissive polarization-independent subtractive color filters exploiting a nanopatch array. *Nano Lett.* **2014**, *14*, 6672–6678. [[CrossRef](#)] [[PubMed](#)]
33. Carrillo, S.G.C.; Trimby, L.; Au, Y.Y.; Nagareddy, V.K.; Rodriguez-Hernandez, G.; Hosseini, P.; Ríos, C.; Bhaskaran, H.; Wright, C.D. A nonvolatile phase-change metamaterial color display. *Adv. Opt. Mater.* **2019**, *7*, 1801782. [[CrossRef](#)]

34. Lee, K.T.; Han, S.Y.; Li, Z.; Baac, H.W.; Park, H.J. Flexible high-color-purity structural color filters based on a higher-order optical resonance suppression. *Sci. Rep.* **2019**, *9*, 14917. [[CrossRef](#)] [[PubMed](#)]
35. Yang, J.H.; Babicheva, V.E.; Yu, M.W.; Lu, T.C.; Lin, T.R.; Chen, K.P. Structural colors enabled by lattice resonance on silicon nitride metasurfaces. *ACS Nano* **2020**, *14*, 5678–5685. [[CrossRef](#)] [[PubMed](#)]
36. Gu, J.; Zhang, Y.; Miao, Y.; Lu, X.; Gao, X. Surface plasma resonance color filter with wider color gamut. *Opt. Commun.* **2021**, *496*, 127127. [[CrossRef](#)]
37. Song, Q.; Miao, Y.; Yan, Q.; Xu, M.; Wang, G.; Gao, X.; Dong, X. High-transmission rotation-angle-dependent plasmonic color filter. *Optik* **2021**, *242*, 167099. [[CrossRef](#)]